

Opto-Electronic Advances

CN 51-1781/TN ISSN 2096-4579 (Print) ISSN 2097-3993 (Online)

High-frequency enhanced ultrafast compressed active photography

Yizhao Meng, Yu Lu, Pengfei Zhang, Yi Liu, Fei Yin, Lin Kai, Qing Yang and Feng Chen

Citation: Meng YZ, Lu Y, Zhang PF, et al. High-frequency enhanced ultrafast compressed active photography. *Opto-Electron Adv* 8, 240180(2025).

<https://doi.org/10.29026/oea.2025.240180>

Received: 31 July 2024; Accepted: 29 October 2024; Published online: 15 January 2025

Related articles

Ultrafast dynamics of femtosecond laser-induced high spatial frequency periodic structures on silicon surfaces

Ruozhong Han, Yuchan Zhang, Qilin Jiang, Long Chen, Kaiqiang Cao, Shian Zhang, Donghai Feng, Zhenrong Sun, Tianqing Jia
Opto-Electronic Science 2024 3, 230013 doi: [10.29026/oes.2024.230013](https://doi.org/10.29026/oes.2024.230013)

Ostensibly perpetual optical data storage in glass with ultra-high stability and tailored photoluminescence

Zhuo Wang, Bo Zhang, Dezhi Tan, Jianrong Qiu
Opto-Electronic Advances 2023 6, 220008 doi: [10.29026/oea.2023.220008](https://doi.org/10.29026/oea.2023.220008)

More related article in Opto-Electronic Journals Group website 



<http://www.ojournal.org/oea>



 OE_Journal



 @OptoElectronAdv



DOI: 10.29026/oea.2025.240180

CSTR: 32247.14.oea.2025.240180

High-frequency enhanced ultrafast compressed active photography

Yizhao Meng¹, Yu Lu^{1*}, Pengfei Zhang¹, Yi Liu¹, Fei Yin², Lin Kai¹,
Qing Yang² and Feng Chen^{1*}

Single-shot ultrafast compressed imaging (UCI) is an effective tool for studying ultrafast dynamics in physics, chemistry, or material science because of its excellent high frame rate and large frame number. However, the random code (R-code) used in traditional UCI will lead to low-frequency noise covering high-frequency information due to its uneven sampling interval, which is a great challenge in the fidelity of large-frame reconstruction. Here, a high-frequency enhanced compressed active photography (H-CAP) is proposed. By uniformizing the sampling interval of R-code, H-CAP capture the ultrafast process with a random uniform sampling mode. This sampling mode makes the high-frequency sampling energy dominant, which greatly suppresses the low-frequency noise blurring caused by R-code and achieves high-frequency information of image enhanced. The superior dynamic performance and large-frame reconstruction ability of H-CAP are verified by imaging optical self-focusing effect and static object, respectively. We applied H-CAP to the spatial-temporal characterization of double-pulse induced silicon surface ablation dynamics, which is performed within 220 frames in a single-shot of 300 ps. H-CAP provides a high-fidelity imaging method for observing ultrafast unrepeatable dynamic processes with large frames.

Keywords: ultrafast compressed imaging; high-frequency enhanced sampling; spectral-temporal transform; transient processes; high-fidelity reconstruction

Meng YZ, Lu Y, Zhang PF et al. High-frequency enhanced ultrafast compressed active photography. *Opto-Electron Adv* 8, 240180 (2025).

Introduction

The development of ultrafast imaging technologies is very valuable for observing ultrafast phenomenon such as laser-induced plasma¹⁻³, interaction between nanoparticles and laser-induced bubbles⁴, or femtosecond laser ablation^{5,6}. The above ultrafast processes have very high time complexity and more than one physical mechanism with different time scales might be concerned in a single ultrafast phenomenon. For example, the visualization of shock wave induced by femtosecond laser can be used

for material analysis⁷, observing the ultrafast cavitation effect of bubbles induced by laser in a liquid containing nanoparticles will have important applications in biological fields such as drug delivery⁸, the comprehensive observation of the ultrafast dynamics such as material phase transition occurring in the ablation area is beneficial to improve the processing results^{9,10}. Therefore, in order not to lose any key information in the whole observation window of the investigation, the implementation of large frame number observation is an indispensable

¹State Key Laboratory for Manufacturing System Engineering and Shaanxi Key Laboratory of Photonics Technology for Information, School of Electronic Science and Engineering, Xi'an Jiaotong University, Xi'an 710049, China; ²School of Mechanical Engineering, Xi'an Jiaotong University, Xi'an 710049, China.

*Correspondence: Y Lu, E-mail: luyu90@xjtu.edu.cn; F Chen, E-mail: chenfeng@mail.xjtu.edu.cn

Received: 31 July 2024; Accepted: 29 October 2024; Published online: 15 January 2025



Open Access This article is licensed under a Creative Commons Attribution 4.0 International License.

To view a copy of this license, visit <http://creativecommons.org/licenses/by/4.0/>.

© The Author(s) 2025. Published by Institute of Optics and Electronics, Chinese Academy of Sciences.

requirement for the current ultrafast imaging technology. The traditional pump-probe technology can only capture one frame at each time and requires that the observed dynamic events must be accurately and repeatedly measured^{11–13}, thus limiting its application in random or unstable ultrafast phenomena. To study the ultrafast process that is difficult to repeat, many single-shot multi-frame active imaging techniques have been developed in recent years^{14–17}. While these methods have achieved effective imaging outcomes, the constraints of the optical system make it be challenging to obtain finer resolved time, higher imaging frame rate, as well as larger frame number at the same time with the time complexity of the observed object increases.

With the development of compressed sensing^{18–20}, to achieve the largest number of acquisition frames, ultrafast compressed imaging technology combined with computational imaging has become a promising method^{21–25}. However, the imaging spatial resolution will decrease with the increase of frame number during reconstruction due to the increase in compression rate. This brings challenges to the observation of ultrafast processes with both high spatial and high time complexity. At present, many advanced imaging methods have improved the spatial resolution by optimizing the optical system to increase the number of encodings^{26,27}, using lossless-encoding^{28,29} or adding prior information^{23,28,30,31}. These methods essentially increase the number of solution conditions when solving the inverse problem of compressed imaging, but each solving condition is not optimized. The structure distribution of code is a very important part of the solution conditions, which has an irreplaceable impact on high-quality reconstruction of large frames. Ultrafast compressed imaging usually uses random code (R-code) to sample the ultrafast process. In the spatial domain, the pixel distribution of R-code will lead to the formation of a large uncoded area, and the acquisition will be flawed³². In the frequency domain, the Fourier transform energy distribution of R-code in high-frequency and low-frequency is the same. The high-frequency information of ultrafast phenomenon will be annihilated in the low-frequency energy of R-code during acquisition, which blurs the high-frequency detail information. Therefore, from the perspective of improving reconstruction fidelity, if the code plays the role of enhancing high-frequency information during acquisition, it will help to solve the problem of high-quality reconstruction of ultrafast compressed imaging.

In this paper, a high-frequency enhanced compressed active photography (H-CAP) is proposed, which encodes the ultrafast process with a uniform sampling interval to enhance high-frequency information. At the same time, the code has randomness and highly satisfies the reconstruction characteristics of compressed sensing. The Fourier transform of the new code shows that the high-frequency energy is much higher than the low-frequency energy, which can greatly reduce the loss of detailed information caused by the low-frequency structural noise. It effectively overcomes the detail blur caused by R-code reconstruction and realizes the high spatial frequency acquisition of ultrafast process. We experimentally demonstrate that the spatial resolution is 8.98 lp/mm at 2.5 mm × 2.5 mm field of view (FOV) with 100 captured frames and the reconstruction fidelity can reach more than 0.84. To demonstrate the wide application ability of H-CAP, we successfully used it to observe the ultrafast dynamics of double-pulse ablation of silicon at a long-time window of 300 ps with 220 frames in a single-shot. The experimental results well prove the superior ability of this technology.

Principle and simulation

Optical setup of H-CAP

In Fig. 1(a), when the temporally shaped pulse acts on the surface of the material by using Lens 5 (L5), the chirped pulse captures this ultrafast process $O(x, y, t)$ through the 4f beam-shrinking system (L1 and microscope objective (MO)). According to the principle of spectral-temporal transform, different wavelengths correspond to different times. The original ultrafast process belongs to a high-dimensional vector (x, y, t three dimensions). The data storage and transmission speed of the acquisition device cannot directly collect the data, so we need to use compressed imaging technology. Based on the principle of compressed sensing, the ultrafast information after spectral-temporal transform needs to be coded firstly for discrete sampling through the magnification system composed of MO and L2. Then, the ultrafast information after code sampling is spectrally modulated horizontally through a grating. Next, CCD records the two-dimensional image after spectral intensity superposition (L3 and L4). Finally, the compressed sensing algorithm is used to reconstruct the image with high-fidelity.

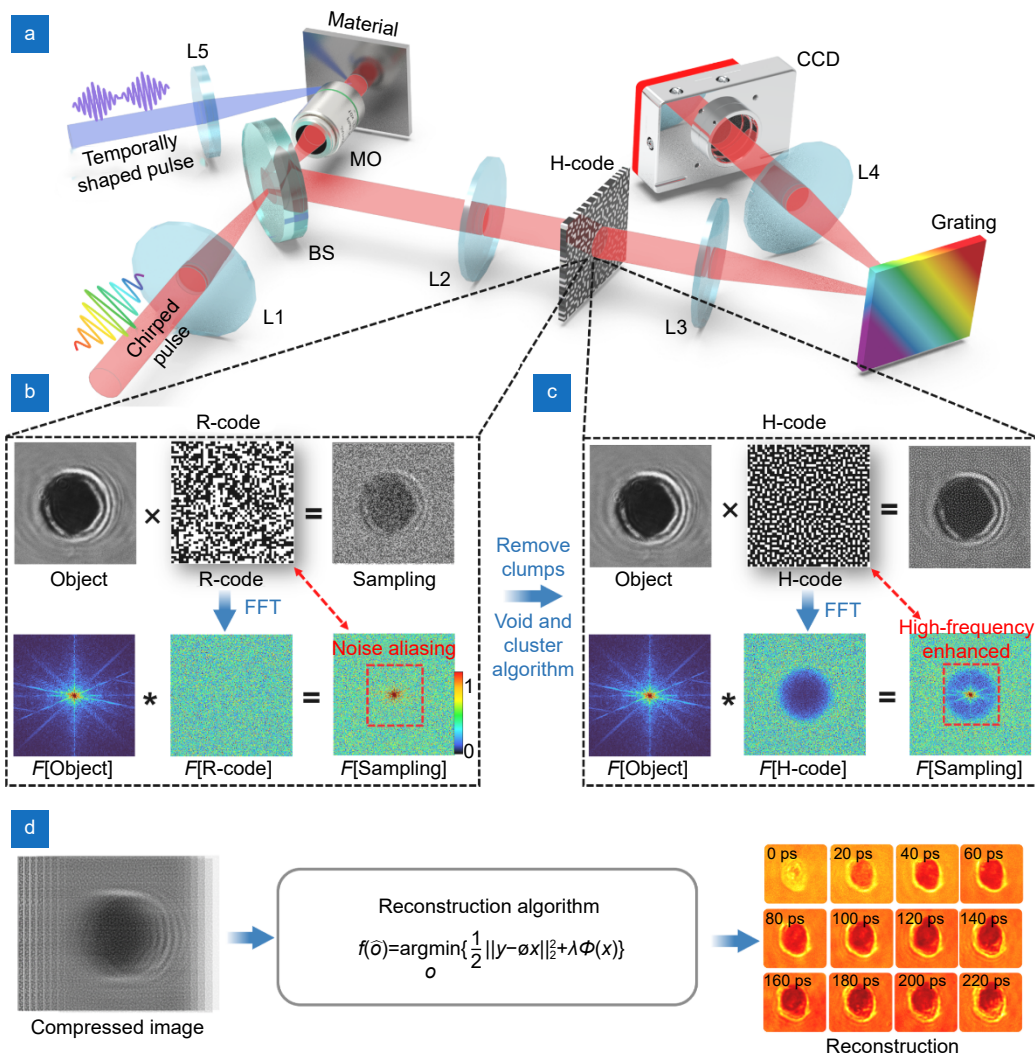


Fig. 1 | The optical setup and principle of high-frequency enhanced compressed active photography (H-CAP). (a) The optical setup of the H-CAP system. (b) The sampling principle of R-code and (c) H-code in the spatial and frequency domain. (d) The ultrafast phenomena are reconstructed from the compressed image by using a reconstruction algorithm.

Principle of H-CAP

We describe the principle of H-CAP in Fig. 1(b) and 1(c). We first analyze the ultrafast phenomenon after encoding by random code (R-code) in the spatial domain and frequency domain respectively (Fig. 1(b)). In the spatial domain, the pixel distribution of R-code commonly used in ultrafast compressed imaging always has black pixels or white pixels clustered together. The aggregation of black pixels will form a large uncoded area, which will cause the loss of information. And the white pixels together will produce redundant samples. It can be seen from the Fig. 1(b) that when the original object is sampled by R-code, the high-frequency detail information of the original object has been lost visually due to the above characteristics of R-code, which is not con-

ducive to the subsequent reconstruction of compressed active photography. In the frequency domain, the energy distribution of R-code in each frequency component is almost the same. The spectrum of the sampled signal is obtained by convoluting the spectrum of the object with the Fourier spectrum of R-code. From the spectrum of the sampled signal, it shows that the high-frequency information of the object will be annihilated in the low-frequency structure of the R-code (in the red box), resulting in the loss of high frequency information. From the principle of sampling, random sampling can eliminate the influence of ‘jaggies’ artifacts on the edge of image compared with uniform sampling, but it also introduces low-frequency structured noise in the acquisition and blurs high-frequency information³³. The clumps (the

area of code aggregation) in the spatial distribution of R-code are important factors that cause high frequency information covered. Therefore, to enhance the high-frequency information of the object, we must eliminate the clumps in the R-code³². Yellott pointed out that spatially uniformly distributed and randomly placed coded pixels can often capture better samples³⁴. Therefore, we use the Void and Cluster method³⁵ (see Supplementary information for details.) to rearrange the pixel distribution of R-code, resulting in a coding matrix with a more uniform sampling interval (Fig. 1(c)). When we use the newly generated code to collect the original object, compared with the sampling results of the R-code, the processed code retains the high-frequency information of the object during sampling. The newly generated code is called high-frequency enhanced random code (H-code). Subsequently, we also analyze the sampling results of H-code in the frequency domain (Fig. 1(c)). In contrast, the high-frequency energy of H-code is much higher than the low-frequency energy. Therefore, the high-frequency component of the object (in the red box) is retained after convolution with the Fourier spectrum of the object. In addition, this code also highly satisfies the reconstruction property of compressed sensing. Due to the high-frequency enhanced function of H-code, when we use the compressed image collected by H-code combined with the compressed sensing algorithm to reconstruct, we can improve the signal-to-noise ratio in the case of large frames acquisition (Fig. 1(d)).

Simulation

To compare the reconstruction ability of H-code and R-code, we first carry out simulation experiments. The simulation object is the three-reflection process of the light, and the number of frames is 200 frames. The idea of high-channel photography is combined during subsequent reconstruction, and the number of channels is 7 (high-channel and image reconstruction are explained in Supplementary information and are illustrated in Fig. 2(a)). Figure 2(b) is the compressed images of 200 frames collected under different codes and corresponding Fourier transform. The dynamic process of H-coded sampling is more uniform in visual effect. From the spectrum of spot track, H-code can effectively retain the high-frequency information of ultrafast process and improve the signal-to-noise ratio. From Fig. 2(c), the light quality reconstructed by H-code is very excellent, and it will not be disturbed by noise in the transmission pro-

cess (yellow dotted arrow). However, due to the mixing of low-frequency and high-frequency information, R-code leads to many unsatisfactory noises in the reconstruction results, which affects the subsequent data analysis. In addition, we integrated the intensity center of 200 frames and compared it with the original data, which obtained a clearer representation, as shown in Fig. 2(d). The data of the light intensity center integrated from the reconstruction result of H-code (yellow scatter) shows excellent results, which is very close to the original motion trajectory of the light (red line). In contrast to the reconstruction results of R-code (blue scatter), the light intensity center fluctuates greatly near the original trajectory, and even some points have seriously deviated from the original trajectory. We also calculate the beam length of the reconstruction results in Fig. 2(c), as shown in Fig. 2(e). The process of the beam length decreasing first and then increasing corresponds to the moment of reflection. Compared with the calculation results of R-code, the results of H-code are closer to the length of the original beam. For the PSNR and SSIM of the reconstruction results in Fig. 2(c), please refer to Fig. S8 in Supplementary information. The results of Fig. S8 show that the reconstruction ability of H-code is much better than that of R-code. Therefore, the simulation results show that the reconstruction results will be greatly improved as the spatial distribution of code tends to be uniform. This is conducive to observing the ultrafast process with high space-time complexity.

Result and discussion

The large frame reconstruction ability of H-CAP

In the experiment of H-CAP, we use the high-channel recording device (see Section 3 in Supplementary information, the detailed experiment parameters are in Section 7) to capture objects. To verify that H-CAP has excellent reconstruction ability under large frames, we perform the characterization of static objects. The imaging system of this experiment is 1:1 imaging. The fineness of the first two groups of objects selected increases in turn. The resolution target of USAF 1951 is chosen as the third group of objects to quantitatively characterize the spatial resolution. Figure 3(a) is the original image of the first two groups of objects. Figure 3(b) is the compressed image of the corresponding object in Fig. 3(a) under 100 frames. (To view the compressed image clearly, we only show the compressed image of one channel here. For

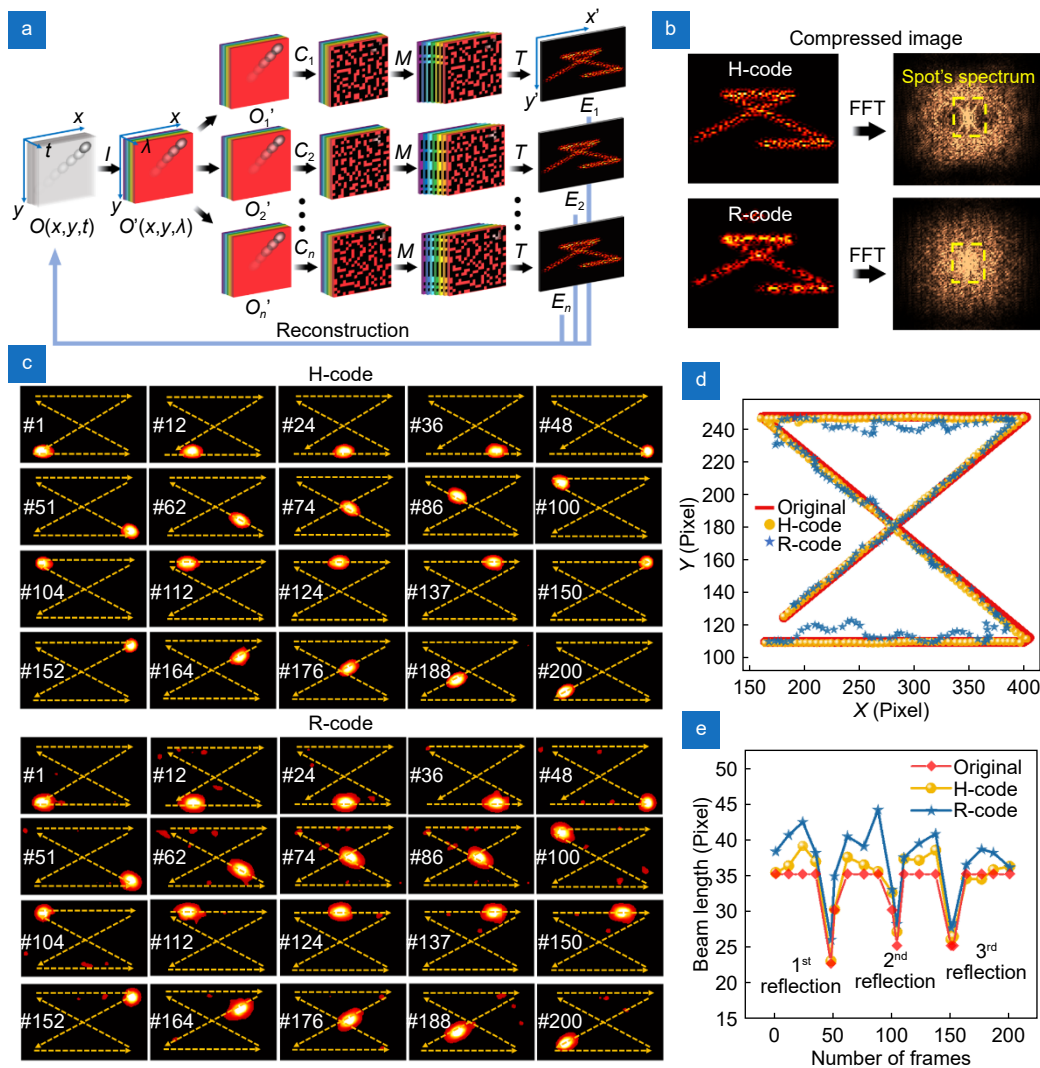


Fig. 2 | Simulation results of H-code and R-code. (a) Forward model of high-channel photography. (b) The compressed images of 200 frames collected under different codes and corresponding Fourier transform. (c) Reconstruction results of light reflection under different codes. (d) The comparison of the light intensity center extracted from the reconstruction results of H-code and R-code with the original data. (e) The beam length calculated according to the reconstruction results of different codes.

compressed images of 7-channel, please see Fig. S10 in Supplementary information.) The object 'Laser' in Fig. 3(b) is the original acquisition direction, and is rotated in Fig. 3(a) and subsequent reconstruction results for ease of comparison. Figure 3(c) shows the comparison of the reconstruction results of H-code and R-code when the number of acquisition frames increases from 40 frames to 100 frames. It can be seen from the Fig. 3(c) that with the increase of the number of frames, the letters in the reconstruction results of H-code can still be clearly distinguished. In contrast, the reconstruction quality of R-code will decrease significantly, and some information of the object will be missing, which will also bring additional reconstruction noise. To more clearly characterize the

H-code still has good reconstruction ability under large frame number acquisition, the correlation between the reconstructed object and the original object is calculated. (This value is used to represent the fidelity.) From the correlation curve of 'UPL' in Fig. 3(d), the reconstruction correlation of H-code only decreases from 0.841 to 0.838 (the decreasing rate is 0.36%) when the number of frames increases from 40 to 100. However, the reconstruction correlation of R-code decreases from 0.818 to 0.795 (the decreasing rate is 2.8%). In other words, when there are a high number of frames, H-code is able to remain the same level of reconstruction quality as with a smaller number of frames. Furthermore, the reconstruction result of H-code consistently outperforms that of R-

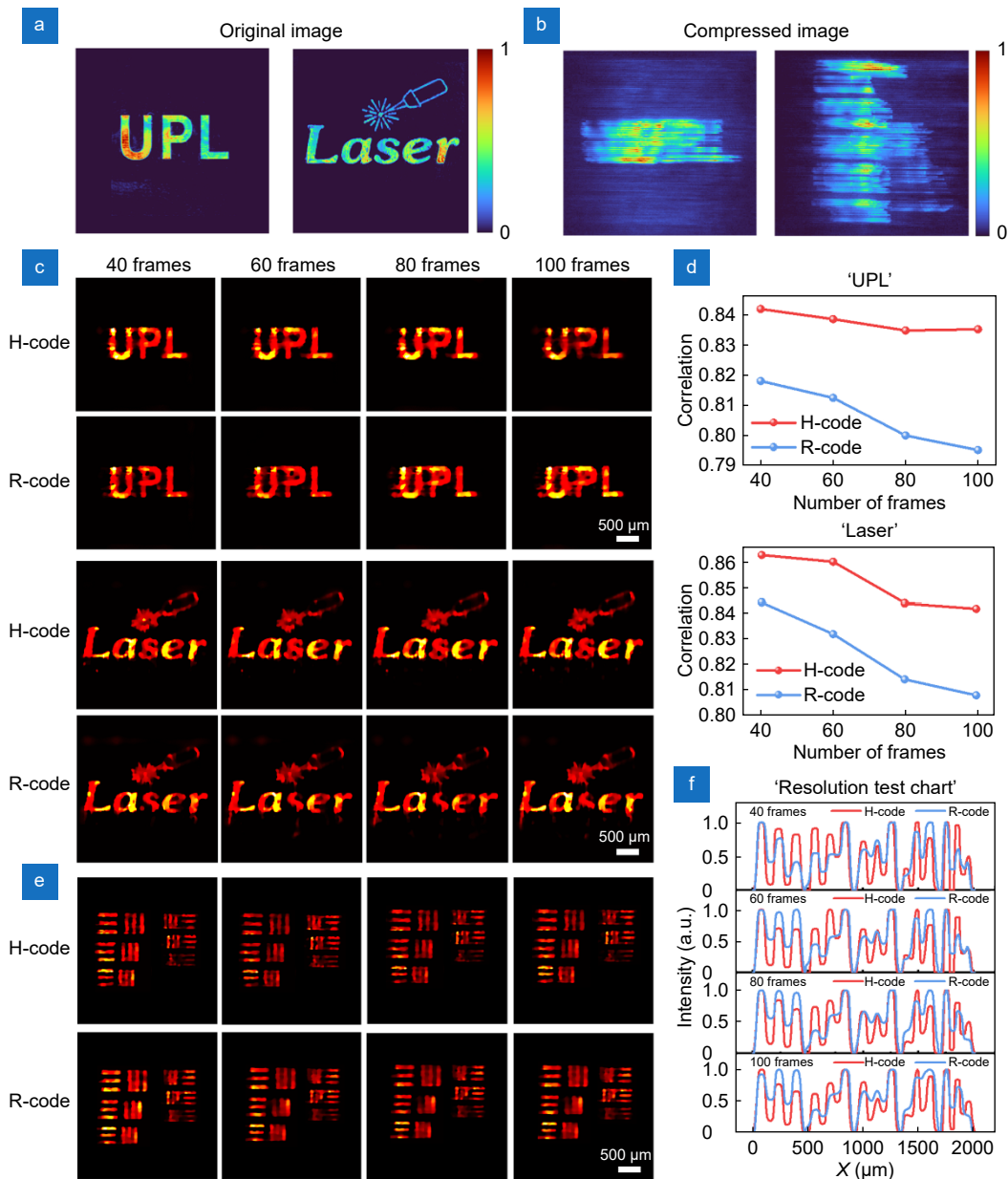


Fig. 3 | Characterization of static experimental results. (a) The original image of the object. (b) The compressed image of the object with 100 frames. (c) Reconstruction results of 'UPL' and 'Laser' under different captured frames. (d) The correlation between the reconstruction result in (c) and the original object. (e) Reconstruction results of the resolution target under different captured frames. (f) The intensity curves of vertical stripes in (e).

code, regardless of the number of frames. From the correlation curve of 'Laser', we can get the same conclusion. The above results show that the fidelity of H-code can reach more than 0.84. Finally, to characterize the spatial resolution of H-code, the reconstruction result of resolution target of USAF 1951 (spatial resolution corresponds to 5.6 lp/mm–10 lp/mm) is obtained, as shown in Fig. 3(e). From the figure, as the number of frames increases, the reconstructed spatial resolution of R-code becomes worse and worse. Under the compression ac-

quisition of 100 frames, the reconstruction result of H-code can be resolved to 8.98 lp/mm, while the random coding can only be resolved to 6.4 lp/mm. Similarly, in order to more intuitively find out the compared result, the intensity curve of the vertical stripes on Fig. 3(e) is made, and the results are shown in Fig. 3(f) (the lines of 10 lp/mm are not represented in the figure). As can be seen, when the number of frames is 100, the peak of the vertical stripe with a spatial resolution of 8.98 lp/mm can be reconstructed and distinguished by H-code. Random

code can only distinguish the peak with a spatial resolution of 6.4 lp/mm. Therefore, it means that the H-CAP has a spatial resolution of 8.98 lp/mm at 100 frames and a field of view of 2.5 mm × 2.5 mm. By adding a microscopy to the imaging system, higher spatial resolution can be obtained.

Imaging of the self-focusing of optical pulses in Kerr medium

Birefringence effect induced by ultrashort laser in optical Kerr medium³⁶ has great applications in all-optical communication³⁷, ultrafast fluorescence measurement³⁸ and ultrafast optical imaging. Femtosecond laser is easy to generate self-focusing effect in Kerr medium due to its high peak power, which changes the focusing character-

istics of the beam. As an experiment to verify the superior dynamic resolution of H-CAP, we observe the self-focusing process of the beam in CS₂. The simple design of the experiment is shown in Fig. 4(a). The pump pulse is focused in CS₂ through an objective lens (Olympus, 5×, NA = 0.1). Only around the region excited by the pump pulse, a chirped pulse with a 45° polarization can pass through the region and be detected by the subsequent polarizer. Finally, the process is recorded by H-CAP. The detailed experiment parameters are in Section 7. Figure 4(b) shows the reconstruction results of H-code and R-code. The total recording time is 22.2 ps, and the number of recorded frames is 50 frames. From the reconstructed process, the result measured by H-code is better. Specifically, there is almost no additional reconstruction

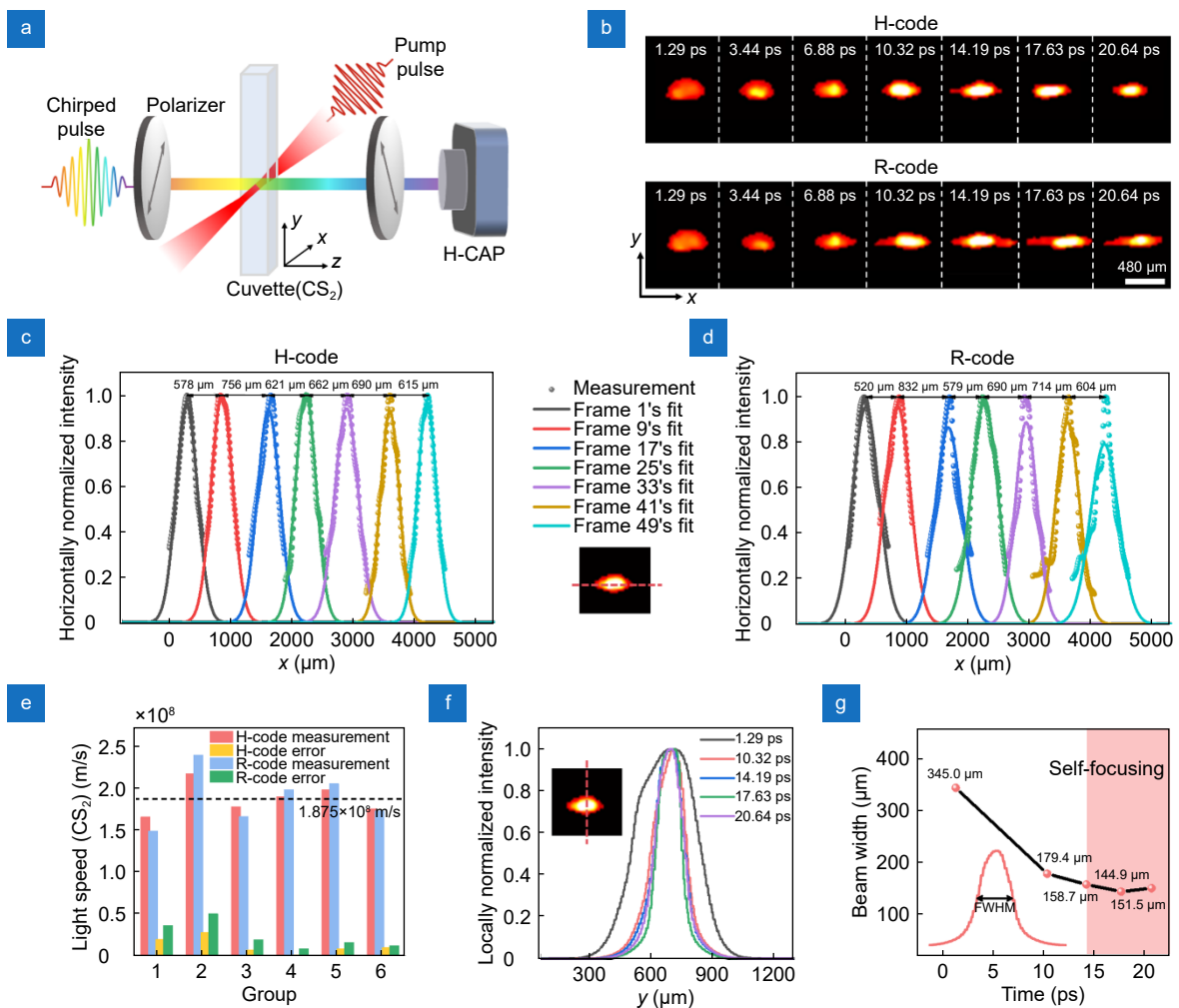


Fig. 4 | Imaging of the self-focusing of optical pulses in Kerr medium. (a) The experimental schematic of optical pulse self-focusing. (b) Reconstruction results of optical pulse self-focusing under different codes. (c) Scatter plot of spots along x direction and corresponding Gaussian fitting curves (every 8 frames in the reconstruction results of H-code). (d) Scatter plot of transverse spot sizes and corresponding Gaussian fitting curves (every 8 frames in the reconstruction results of R-code). (e) The velocity of beam in CS₂ is calculated according to (c) and (d). (f) The intensity curves of the spot along the y direction. (g) The variation of beam width with travel time (according to the full width at half maximum (FWHM) of the curve in (f)). The red box indicates the self-focusing area.

noise on the motion path of the beam, and the shape contour of the beam will not be distorted or affected by the beam at other times. For a clearer comparison, we first qualitatively characterize the transverse size of the spot (x direction). We select a picture every 8 frames in the reconstruction results to perform Gaussian fitting on the transverse size of the spot, as shown in Fig. 4(c) and 4(d). From the comparison results, the scatter distribution extracted from the measurement results of H-code is more consistent with the Gaussian distribution, while there are many offset points in the results of R-code measurement. To quantitatively illustrate the better reconstruction performance of H-code, we calculate the speed of the light in CS₂ according to the moving distance of each 8 frames, which are shown in Fig. 4(e) (the method of calculation is in Supplementary information). Since the refractive index of CS₂ is 1.6, the theoretical value of the moving speed of the spot in CS₂ is calculated to be 1.875×10^8 m/s. From Fig. 4(e), it can be clearly seen that the calculation result based on H-code measurement is closer to the theoretical value. In addition, we analyze the error between the measurement results and the theoretical values. Compared with R-code, the measurement results of H-code can effectively decrease the measurement error double and significantly improve the quality of the measurement results.

Based on the above analysis results, we selected five moments from the H-code measurement results in Fig. 4(b) to quantitatively characterize the self-focusing effect. By extracting the longitudinal size of the spot (y direction), the intensity of the spot along the y direction in Fig. 4(f) and the width of the spot in Fig. 4(g) are obtained. In the traditional linear focusing phenomenon, the longitudinal size of the spot changes continuously and diverges immediately after passing through the focus. The self-focusing experiments of the beam are all measured near the focus of the objective lens. It can be seen from Fig. 4(f) and 4(g), the size of the spot does not change significantly within about 10 ps, which is different from the phenomenon of linear focusing, indicating that the pump pulse has a self-focusing effect in CS₂. Through the self-focusing effect of light pulse in Kerr medium, we verify that H-CAP has the superior performance of reconstructing dynamic process.

Double-pump pulse induced ultrafast ablation process of silicon surface

Temporally shaped pulses can induce different mecha-

nisms with materials due to their unique time characteristics, so that some decisive physical processes can be better controlled^{39,40}. Here, we use the H-CAP imaging system to observe the ultrafast process of double-pump pulse ablation of silicon surface. On the time scale of hundreds of picoseconds, there are abundant physical phenomena when femtosecond laser interacts with materials, such as the ionization of free electrons, the phase transition of materials, etc. To achieve an approximately complete observation of the phase transition process of femtosecond laser ablation of silicon surface, we choose the observation time window is 300 ps in this experiment. (Optical Kerr switch is used to measure the corresponding relationship between the wavelength and time of the chirped pulse. See the Supplementary information for a detailed description.) The specific optical path and details of double pulse ablation are shown in the Section 7 of Supplementary information.

Figure 5(a–c) shows the dynamic process of the double-pulse ablation of silicon surface captured by H-CAP at the imaging speed of 0.74 THz and the acquisition frame number of 220 frames in a single-shot. The number of acquisition frames in this experiment is determined by the spectral width of the chirped pulse used (it is close to the maximum spectral range available) and the linear dispersion of the grating on the CCD's adjacent pixels in the compressive imaging system. The reconstruction results when the inter-pulse delay time τ is 0 ps, 6.7 ps and 13.3 ps are shown in the figure. The single pulse energy is 7 μ J. With the increase of τ , the ablation enhancement effect caused by the double-pulse becomes more and more obvious. This phenomenon occurs due to the presence of a significant quantity of free electrons in the excited silicon during this delay range, resulting in heightened interaction with the subsequent sub-pulse. To further analyze the reconstruction results, we measured the relative reflectivity curve of the excitation region's center over time with varying pulse delays, as depicted in Fig. 5(d). The dynamic change of relative reflectivity can not only reflect the change of plasma density during the interaction between laser and material, but also understand the change of material state. The ultrafast dynamics at $\tau = 0$ ps is firstly analyzed. It can be seen from Fig. 5(d) that in the initial 40 ps of ablation (region I), the relative reflectivity shows a downward trend and decreases to a negative value. This stage indicates that the laser-induced strong ionization increases the surface temperature of the silicon material. The structure of the

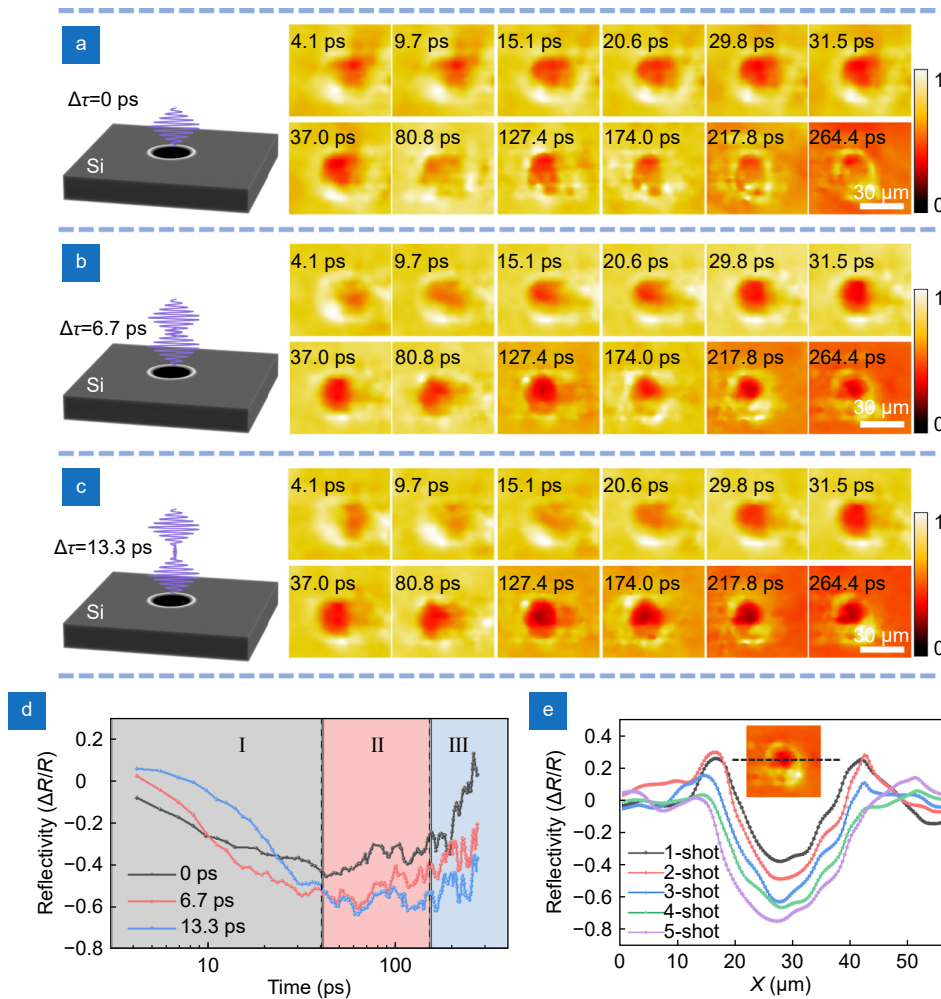


Fig. 5 | Double-pump pulse induced ultrafast ablation process of silicon surface. (a–c) The reconstructed dynamic process of the double-pulse ablation of silicon surface when the inter-pulse delay time τ is 0 ps, 6.7 ps and 13.3 ps. (d) The curves of the relative reflectivity of the center of the excitation region over time under different pulse delay. (e) The change on the depth of the ablation area with the number of shots when the delay between pulses is 6.7 ps and the observation time is 260 ps.

surface melts and gradually generates liquid phase material, which enhances the absorption of light⁴¹. In the range of 40 ps to 150 ps (region II), the relative reflectivity remains basically unchanged. The reason is lattice heat conduction, the liquid phase on the surface of the material remains at a high temperature, preventing the change of reflectivity. At 150 ps–300 ps (region III), the liquid gradually cools with time, the absorption capacity of light is weakened, so the relative reflectivity begins to rise⁴². When the delay between pulses begins to increase, the relative reflectivity curve changes. Due to the delayed excitation of the double pulse, when the second pulse has not yet interacted with the material, the first pulse causes the surface of the excitation region to change slowly because the energy is only half of the double-pulse. When the second pulse reaches the surface, the

reflectivity decreases rapidly. These phenomena can be directly seen from region I. In addition, we also observed from region II that the minimum value of relative reflectivity will fall to a lower point at a new time point when the inter-pulse delay increases, and the upward trend of reflectivity in region III is also smaller. This phenomenon is due to the dense plasma generated by the first pulse on the surface, which changed the instantaneous local characteristics of the material^{43,44}. The plasma carried out a light field reorganization on the second pulse. Therefore, the energy of the second pulse can be deposited into a deeper material space, which effectively improves the ablation effect. Ultimately, we measured the variation in the depth of the ablation area in relation to the number of shots under the condition of a 6.7 ps delay and an observation time of 260 ps. From Fig. 5(e),

as the number of pulses accumulates, the minimum reflectivity of the ablation region decreases from -0.38 to -0.75 , and the full width at half maximum of the ablation region increases from $10.5\ \mu\text{m}$ to $20.3\ \mu\text{m}$. This phenomenon is very consistent with the actual process of laser-matter interaction. The ultrafast phenomenon that the physical mechanism of different time windows change is captured by H-CAP system. It means that the high-precision imaging ability of H-CAP is helpful to study the ultrafast dynamic process of femtosecond laser induced materials.

Discussion

H-CAP improves the problem of high-frequency information loss caused by R-code, which is very helpful for the visualization of unrepeatable ultrafast phenomena. In recent years, some work on ultrafast compressed imaging has also proposed mask optimization methods. For example, Yang et al.⁴⁵ optimized the coding structure by genetic algorithm. The method is to obtain the optimized code through genetic algorithm firstly, and the second is to use the optimized code to improve the quality of image reconstruction. That is, the whole process needs to measure the ultrafast phenomenon twice. For predictable or repeatable ultrafast processes, this method has relatively high reconstruction fidelity. H-code is used to collect the whole ultrafast process, and the coding structure does not change with the change of the observed object. Therefore, the H-CAP system is more advantageous for unpredictable ultrafast phenomena. In addition, Marquez M et al.⁴⁶ combined the deep learning method to optimize the coding structure under the guidance of the CUF's sensing geometry and the spatiotemporal characteristics of the training data. The coding structure has a uniform pixel intensity distribution and reduces low-frequency energy. Compared with H-code, it has a higher sampling rate and can obtain a higher dynamic range. However, the energy distribution of the Fourier spectrum of H-code is approximately isotropic, which can achieve global high-frequency enhancement of the reconstructed image.

The frame interval of H-CAP is defined as the reciprocal of the imaging speed. The temporal resolution depends on the spectral bandwidth of the illumination light used and the group delay dispersion^{47,48}. If the spectral bandwidth of the illumination light is reduced, the time resolution obtained in the same observation time window will decrease. This is a trade-off between observing

time and the time resolution. In the experiment of double-pulse ablation of silicon surface, the spectral bandwidth of the illumination light used is $22.8\ \text{nm}$, and the corresponding time resolution is $3.6\ \text{ps}$ (frame interval is $1.4\ \text{ps}$) under the observation time window of $300\ \text{ps}$. Future research can broaden the available spectrum bandwidth range to improve the time resolution in the same time window.

In addition, H-CAP needs to consider some issues. First, the sampling rate of H-code used in this work is only 33%. There will be many inevitable noises for detection with weak light. Second, although H-code has the ability to enhance high-frequency information, its Fourier spectrum also has a cutoff frequency in the high frequency band and cannot be infinitely extended to any region of the high frequency. A feasible solution is to start with the method of generating H-code, taking into account high sampling rate and high reconstruction fidelity. Another limitation of H-CAP is that the aberration of the whole system determines the pixel size of the coding element ($30\ \mu\text{m}$), which also limits the spatial resolution. For this problem, we need to start with the optimization design of the optical system, which is expected to ensure the acquisition of high-quality coded images and compressed images.

Conclusions

In summary, we use high-frequency enhanced compressed active photography (H-CAP) technology to achieve large frame number observation and high-fidelity reconstruction of ultrafast processes. By using the code with uniform pixel distribution and random placement, the high-frequency detail information is retained during the sampling of the ultrafast process, and the low-frequency structured noise is greatly reduced. Through static experiments, we prove that the H-CAP has a spatial resolution of $8.98\ \text{lp/mm}$ at 100 frames in a field of view of $2.5\ \text{mm} \times 2.5\ \text{mm}$ and the reconstruction fidelity can reach more than 0.84. In addition, we also prove the superior dynamic reconstruction ability of H-CAP through the self-focusing phenomenon of the beam in the Kerr medium. Finally, we use H-CAP to observe the ultrafast dynamic process of double-pulse ablation of silicon surface in a long-time window of $300\ \text{ps}$ with 220 frames. This technique solves the problem that the pixel distribution of R-code will lead to information loss and redundancy when collecting images in compressed ultrafast imaging, which is of great help to observe the ultra-

fast process with higher spatial complexity. In the future, we can also design related algorithms that match the technology to further improve the quality of reconstruction. The large-frame observation and high-fidelity reconstruction capabilities of H-CAP have very important application prospects in irreversible dynamics such as ultrafast laser-matter interaction, ultrafast light field measurement or ultrafast demagnetization.

References

- Couairon A, Mysyrowicz A. Femtosecond filamentation in transparent media. *Phys Rep* **441**, 47–189 (2007).
- Balachninaït O, Skruibis J, Matijošius A et al. Temporal and spatial properties of plasma induced by infrared femtosecond laser pulses in air. *Plasma Sources Sci Technol* **31**, 045001 (2022).
- Liu XL, Lu X, Liu X et al. Tightly focused femtosecond laser pulse in air: from filamentation to breakdown. *Opt Express* **18**, 26007–26017 (2010).
- Bhuyan MK, Soleilhac A, Somayaji M et al. High fidelity visualization of multiscale dynamics of laser-induced bubbles in liquids containing gold nanoparticles. *Sci Rep* **8**, 9665 (2018).
- Ivanov DS, Zhigilei LV. Combined atomistic-continuum modeling of short-pulse laser melting and disintegration of metal films. *Phys Rev B* **68**, 064114 (2003).
- Garcia-Lechuga M, Siegel J, Hernandez-Rueda J et al. Femtosecond laser ablation of dielectric materials in the optical breakdown regime: expansion of a transparent shell. *Appl Phys Lett* **105**, 112902 (2014).
- Kasparian J, Rodriguez M, Méjean G et al. White-light filaments for atmospheric analysis. *Science* **301**, 61–64 (2003).
- Ashiq MGB, Saeed MA, Tahir BA et al. Breast cancer therapy by laser-induced Coulomb explosion of gold nanoparticles. *Chin J Cancer Res* **25**, 756–761 (2013).
- Costache F, Reif J. Femtosecond laser induced Coulomb explosion from calcium fluoride. *Thin Solid Films* **453–454**, 334–339 (2004).
- Carrasco-García I, Vadiño JM, Javier Laserna J. Visualization of surface transformations during laser ablation of solids by femtosecond pump-probe time-resolved microscopy. *Spectrochim Acta Part B At Spectrosc* **113**, 30–36 (2015).
- Fang R, Vorobyev A, Guo CL. Direct visualization of the complete evolution of femtosecond laser-induced surface structural dynamics of metals. *Light Sci Appl* **6**, e16256 (2017).
- Wang QS, Jiang L, Sun JY et al. Structure-mediated excitation of air plasma and silicon plasma expansion in femtosecond laser pulses ablation. *Research* **2018**, 5709748 (2018).
- Zewail AH. Laser femtochemistry. *Science* **242**, 1645–1653 (1988).
- Ehn A, Bood J, Li ZM et al. FRAME: femtosecond videography for atomic and molecular dynamics. *Light Sci Appl* **6**, e17045 (2017).
- Zeng XK, Zheng SQ, Cai Y et al. High-spatial-resolution ultrafast framing imaging at 15 trillion frames per second by optical parametric amplification. *Adv Photonics* **2**, 056002 (2020).
- Ding PP, Qi DL, Yao YH et al. Single-shot polarization-resolved ultrafast mapping photography. *Sci Bull* **68**, 473–476 (2023).
- Nakagawa K, Iwasaki A, Oishi Y et al. Sequentially timed all-optical mapping photography (STAMP). *Nat Photonics* **8**, 695–700 (2014).
- Donoho DL. Compressed sensing. *IEEE Trans Inf Theory* **52**, 1289–1306 (2006).
- Yuan X, Brady DJ, Katsaggelos AK. Snapshot compressive imaging: theory, algorithms, and applications. *IEEE Signal Process Mag* **38**, 65–88 (2021).
- Yuan X, Wu ZL, Luo T. Coded aperture snapshot spectral imager. In Liang JY. *Coded Optical Imaging* 533–547 (Springer, Cham, 2024).
- Lu Y, Wong TTW, Chen F et al. Compressed ultrafast spectral-temporal photography. *Phys Rev Lett* **122**, 193904 (2019).
- Liu JD, Marquez M, Lai YM et al. Swept coded aperture real-time femtophotography. *Nat Commun* **15**, 1589 (2024).
- Wang P, Wang LV. Single-shot reconfigurable femtosecond imaging of ultrafast optical dynamics. *Adv Sci* **10**, 2207222 (2023).
- Liang JY, Zhu LR, Wang LV. Single-shot real-time femtosecond imaging of temporal focusing. *Light Sci Appl* **7**, 42 (2018).
- Tang HC, Men T, Liu XL et al. Single-shot compressed optical field topography. *Light Sci Appl* **11**, 244 (2022).
- Meng YZ, Liu Y, Yin F et al. High-channel spectral-temporal active recording (H-STAR) for femtosecond scenes observation in a single-shot. *ACS Photonics* **11**, 419–427 (2024).
- Yang CS, Qi DL, Liang JY et al. Compressed ultrafast photography by multi-encoding imaging. *Laser Phys Lett* **15**, 116202 (2018).
- Jing JC, Wei XM, Wang LV. Spatio-temporal-spectral imaging of non-repeatable dissipative soliton dynamics. *Nat Commun* **11**, 2059 (2020).
- Liang JY, Ma C, Zhu LR et al. Single-shot real-time video recording of a photonic Mach cone induced by a scattered light pulse. *Sci Adv* **3**, e1601814 (2017).
- Zhu LR, Chen YJ, Liang JY et al. Space- and intensity-constrained reconstruction for compressed ultrafast photography. *Optica* **3**, 694–697 (2016).
- Wang P, Liang JY, Wang LV. Single-shot ultrafast imaging attaining 70 trillion frames per second. *Nat Commun* **11**, 2091 (2020).
- McCool M, Fiume E. Hierarchical Poisson disk sampling distributions. In *Proceedings of the Conference on Graphics Interface '92* 94–105 (Morgan Kaufmann Publishers Inc., 1992)
- Cook RL. Stochastic sampling in computer graphics. *ACM Trans Graph* **5**, 51–72 (1986).
- Yellott JI. Spectral consequences of photoreceptor sampling in the rhesus retina. *Science* **221**, 382–385 (1983).
- Ulichney RA. Void-and-cluster method for dither array generation. *Proc SPIE* **1913**, 332–343 (1993).
- Wang L, Ho PP, Liu C et al. Ballistic 2-D imaging through scattering walls using an ultrafast optical Kerr gate. *Science* **253**, 769–771 (1991).
- Leuthold J, Koos C, Freude W. Nonlinear silicon photonics. *Nat Photonics* **4**, 535–544 (2010).
- Wang HY, De Mello Donegá C, Meijerink A et al. Ultrafast exciton dynamics in CdSe quantum dots studied from bleaching recovery and fluorescence transients. *J Phys Chem B* **110**, 733–737 (2006).
- Chen ZC, Jiang L, Lian YL et al. Enhancement of ablation and ultrafast electron dynamics observation of nickel-based superal-

- loy under double-pulse ultrashort laser irradiation. *J Mater Res Technol* **21**, 4253–4262 (2022).
40. Chowdhury IH, Xu XF, Weiner AM. Ultrafast double-pulse ablation of fused silica. *Appl Phys Lett* **86**, 151110 (2005).
 41. Lian YL, Jiang L, Sun JY et al. Ultrafast quasi-three-dimensional imaging. *Int J Extrem Manuf* **5**, 045601 (2023).
 42. Feng T, Chen G, Han HN et al. Femtosecond-laser-ablation dynamics in silicon revealed by transient reflectivity change. *Micro-machines* **13**, 14 (2021).
 43. Zhao X, Shin YC. Ablation enhancement of silicon by ultrashort double-pulse laser ablation. *Appl Phys Lett* **105**, 111907 (2014).
 44. Kudryashov SI, Samokhvalov AA, Golubev YD et al. Dynamic all-optical control in ultrashort double-pulse laser ablation. *Appl Surf Sci* **537**, 147940 (2021).
 45. Yang CS, Qi DL, Wang X et al. Optimizing codes for compressed ultrafast photography by the genetic algorithm. *Optica* **5**, 147–151 (2018).
 46. Marquez M, Balistreri G, Morandotti R et al. Metalens-based compressed ultracompact femtophotography: analytical modeling and simulations. *Ultrafast Sci* **4**, 0052 (2024).
 47. Tang HC, Marquez M, Men T et al. Temporal resolution of ultrafast compressive imaging using a single-chirped optical probe. *Opt Lett* **48**, 6080–6083 (2023).
 48. Sun FG, Jiang ZP, Zhang XC. Analysis of terahertz pulse mea-

surement with a chirped probe beam. *Appl Phys Lett* **73**, 2233–2235 (1998).

Acknowledgements

This work was supported by the National Science Foundation of China (No. 12127806, No. 62175195 and No. 12304382), the International Joint Research Laboratory for Micro/Nano Manufacturing and Measurement Technologies.

Author contributions

Y. Z. M. and Y. L. designed and built the system and conducted all the experiments. Y. Z. M. and P. F. Z. gathered experimental data. Y. Z. M. and Y. L. developed the algorithm. F. Y. designed and purchased coded apertures. Y. Z. M., L. K., and Q. Y. analyzed the data and drafted the manuscript. F. C. supervised the project and provided fund support. All authors were involved in revising the manuscript.

Competing interests

The authors declare no competing financial interests.

Supplementary information

Supplementary information for this paper is available at <https://doi.org/10.29026/oea.2025.240180>



Scan for Article PDF